

Transmission in graphene through tilted barrier in laser field

Rachid El Aitouni,¹ Miloud Mekkaoui,¹ and Ahmed Jellal^{1,2,*}

¹Laboratory of Theoretical Physics, Faculty of Sciences,
Chouaib Doukkali University, PO Box 20, 24000 El Jadida, Morocco

²Canadian Quantum Research Center, 204-3002 32 Ave Vernon, BC V1T 2L7, Canada

We study the transmission of Dirac fermions in graphene through a tilted barrier potential in the presence of a laser field. By using Floquet theory, we solve the Dirac equation and then obtain the energy spectrum. The boundary conditions together with the transfer matrix method allow us to determine the transmission probabilities corresponding to all energy bands. For numerical purposes, we only study the central band $l = 0$ and the two first side bands $l = \pm 1$ under various conditions. It has been discovered that the laser field and potential influence the amplitude and shape of the transmission probabilities. In fact, different oscillations are observed, the Klein effect is still present, and the transmission of all bands is almost zero inside the barrier.

PACS numbers: 78.67.Wj, 05.40.-a, 05.60.-k, 72.80.Vp

KEYWORDS: Graphene, laser field, barrier potential, transmission probability.

I. INTRODUCTION

Graphene is one of the few two-dimensional materials that is made up of carbon atoms that form a hexagonal structure in the shape of a honeycomb [1]. The thickness of which does not exceed the thickness of an atom. It has incredible mechanical, electronic, optical, thermal, and chemical properties [2], as well as extremely high mobility. The speed of its electrons is 300 times less than the speed of light [3]. Because of its speed, the researchers consider its electrons to be massless Dirac fermions. It is one of the most powerful conductors of electricity and heat, which has started to be used in technology industries [4–6]. It replaces ordinary semiconductors such as silicon to manufacture electronic components, solar panels, and touch displays. The Hamiltonian describing the graphene properties is a relativistic Dirac Hamiltonian, resulting within the framework of the tight-binding model [3]. The eigenvalue equation resolution reveals that the Brillouin zone is delimited by six Dirac points, which are represented by two non-equivalent points K and K' , each corresponding to two atoms of the pattern in the direct lattice. In addition, the energy is a linear dispersion relation in the vicinity of the Dirac points [7], which is similar to a cone, i.e., the valence and the conduction band are tangent at the Dirac points. As a result, the electrons inside graphene can easily jump from the valence band to the conduction band. This is the problem that delays its use. The zero gap between these two bands prompted many researchers to look for ways to create a gap between them. Among the methods proposed are: confining the charge to the surface in systems composed of multi-layered graphene [8], deformation of the graphene sheet [3, 9–12], and application of different fields like electric, magnetic, or laser fields [13–17].

Laser technology has become a powerful tool for the advancement of investigations into graphene. Indeed, several studies have been conducted on the effect of a linear or circular laser field on the mobility of Dirac fermions in graphene [18–20], demonstrating that the laser can create a band gap in the energy spectrum. On the other hand, the tunneling effect has been studied for Dirac fermions in graphene subjected to a linear vector potential [13, 21]. Here, the infinite mass boundary condition reduced our 2D Dirac equation to a massively effective 1D Dirac equation with an effective mass equal to the quantized transverse momentum. Note that the transmission probabilities of Dirac fermions through different barriers are studied. In particular, rectangular barriers [13] and inclined barrier [21] all show that the transmissions are not null even if the incident energies are lower than the barrier height, which is called the Klein's tunnel effect [22, 23]. Barrier potentials in conjunction with laser fields have also been investigated [15, 16, 24] and potential oscillations over time [25]. As a result, it was discovered that side bands $l\hbar\omega$ ($l = 0, \pm 1, \dots$) were added to the energy spectrum, giving rise to an infinite number of transmission probabilities.

We investigate how Dirac fermions in graphene can pass through a slanted barrier potential in the presence of a laser field. The Dirac equation is solved using Floquet theory, and the energy spectrum is then obtained. The transfer matrix approach and boundary conditions enable us to ascertain the transmission probabilities corresponding to all energy bands. Under different conditions, only the central band $l = 0$ and the two first side bands $l = \pm 1$ are examined numerically. It has been found that the amplitude and shape of the transmission probabilities are affected

* a.jellal@ucd.ac.ma

by the laser field and potential. In reality, a variety of oscillations are seen inside the barrier, the Klien effect is still evident, and the transmission of all bands is practically nonexistent.

This paper is organized as follows. In Sec. II, we set the mathematical formalism based on the Hamiltonian describing the present system. By solving the eigenvalue equation, we will be able to explicitly determine the eigenspinors in all regions composing the system under consideration. These solutions will allow us, in Sec. III, to use the boundary conditions at interfaces, and by employing the transfer matrix approach, we will calculate all transmission channels resulting from the oscillating barrier, which causes the energy subbands $l\hbar\omega$ ($l = 0, \pm 1, \dots$). In Sec. IV, we will numerically analyze our results by plotting the three first transmission probabilities as a function of the physical parameters. Finally, we conclude our work.

II. THEORETICAL MODE

We consider a graphene sheet subjected to a tilted potential $V(x)$ and irradiated by a linear polarization monochromatic laser $A(t)$ over a finite region of length d , while the other two regions are pure graphene as depicted in Fig. 1.

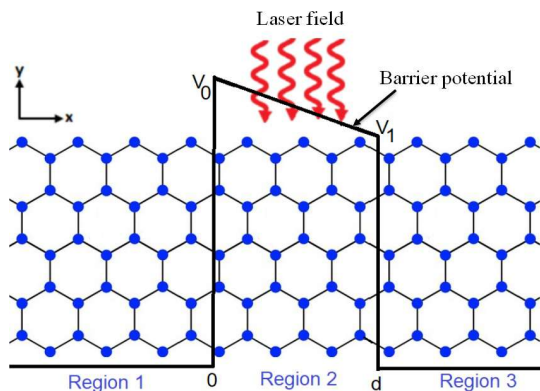


FIG. 1. Schematic diagram of a graphene sheet electrostatic inclined barrier irradiated by a monochromatic laser field over a finite region of length d .

The Hamiltonian describing the system is given by

$$H = v_F \vec{\sigma} \cdot [\vec{p} - e\vec{A}(t)] + V(x)\mathbb{1}_2 \quad (1)$$

where v_F is the Fermi velocity $\approx 10^6 m/s$, $\sigma_{x,y}$ are the Pauli matrices, $\vec{p} = -i\hbar(\partial_x, \partial_y)$ is two dimensional momentum, e being the electronic charge and $\mathbb{1}_2$ is 2×2 identity matrix. The scalar potential $V(x)$ varies along the x -axis and is represented by

$$V(x) = \begin{cases} -\beta x + V_0, & 0 < x < d \\ 0, & \text{otherwise} \end{cases} \quad (2)$$

which can be produced by two identical plates located at $x = 0$ and $x = d$, where $\beta = \frac{V_0 - V_1}{d}$ and $V_0 > V_1$. In the dipole approximation [26], the vector potential $\vec{A}(t)$ of the laser field is given by

$$\vec{A}(\vec{r}, t) = (0, A_0 \cos(\omega t), 0, t) \quad (3)$$

where $A_0 = \frac{E}{\omega}$ is the laser field amplitude. An electric field \vec{E} with frequency ω and amplitude F can generate such a potential. Indeed, we can write

$$\vec{E} = -\frac{\partial}{\partial t} \vec{A}(t) = \vec{F} \sin(\omega t). \quad (4)$$

The present system is composed of three regions labeled $j = 1, 2, 3$. Then we have to determine the solutions of the energy spectrum in each region using the eigenvalue equation

$$[v_F \sigma_x p_x + v_F \sigma_y (p_y - eA(t)) + V_j(x)\mathbb{1}_2] \Psi_j(x, y, t) = i\hbar \frac{\partial}{\partial t} \Psi_j(x, y, t). \quad (5)$$

Since the system has a finite width R , then one can use the boundary conditions at $y = 0, R$

$$\Psi_1(x, 0, t) = -\Psi_2(x, 0, t) \quad (6)$$

$$\Psi_1(x, R, t) = -\Psi_2(x, R, t) \quad (7)$$

to quantize the transverse wave vector

$$k_y = \frac{\pi}{R} \left(n + \frac{1}{2} \right), \quad n = 0, \pm 1, \dots \quad (8)$$

The laser field is considered to oscillate periodically in time, which has an effect on the behavior of the wave function and the energy band. Consequently, the Floquet approximation [27] should be taken into account to determine the solutions of the eigenvalue equation. The eigenspinors can also be separated in coordinates because the Hamiltonian is invariant along the y -direction. Combining all of these, we can write the eigenspinors solution of (5) as

$$\Psi_j(x, y, t) = (\psi_{j1}(x), \psi_{j2}(x))^T e^{ik_y y} \phi_0(t) e^{-iEt} \quad (9)$$

where E denotes the Floquet energy and $\phi_0(t)$ varies over time, $\phi_0(t + \tau) = \phi_0(t)$, τ denotes the laser field period and t denotes transpose. As a result, (5) provides us with

$$\left(-i \frac{\partial}{\partial x} - i \left(k_y - \frac{F}{\omega} \cos(\omega t) \right) \right) \psi_{j2}(x) \phi_0(t) = i \psi_{j1}(x) \frac{\partial \phi_0(t)}{\partial t} + (E - V(x)) \psi_{j1}(x) \phi_0(t) \quad (10)$$

$$\left(-i \frac{\partial}{\partial x} + i \left(k_y - \frac{F}{\omega} \cos(\omega t) \right) \right) \psi_{j1}(x) \phi_0(t) = i \psi_{j2}(x) \frac{\partial \phi_0(t)}{\partial t} + (E - V(x)) \psi_{j2}(x) \phi_0(t) \quad (11)$$

where dimensionless quantities are introduced $A \rightarrow AFt_0$, $(x, y) \rightarrow (x, y)d_0$, $k_y \rightarrow k_y/d_0$, $V(x) \rightarrow V(x)E_0$, $E \rightarrow EE_0$, $t \rightarrow tt_0$ and $\omega \rightarrow \omega\omega_0$, with the length $d_0 = \sqrt{\frac{\hbar v_F}{eF}}$, energy $E_0 = \frac{\hbar v_F}{d_0}$ and time $t_0 = \frac{d_0}{v_F}$ scales.

It is worth noting that there are only two differential equations and three unknown wave functions, $\psi_{j1}(x)$, $\psi_{j2}(x)$, and $\phi_0(t)$. To overcome this situation, we apply the iterative method as a first approximation by supposing that ψ_{21} and ψ_{22} satisfy the Dirac equation in region 2 without laser irradiation. As a result, (10-11) becomes

$$\frac{F}{w} \cos(\omega t) \psi_{22}(x) \phi_0(t) = \psi_{21}(x) \frac{\partial}{\partial t} \phi_0(t) \quad (12)$$

$$- \frac{F}{w} \cos(\omega t) \psi_{21}(x) \phi_0(t) = \psi_{22}(x) \frac{\partial}{\partial t} \phi_0(t). \quad (13)$$

From these we end up with the second order differential equation

$$\frac{\partial^2 \phi_0(t)}{\partial t^2} + \omega \tan(\omega t) \frac{\partial \phi_0(t)}{\partial t} + \frac{F^2}{\omega^2} \cos^2(\omega t) \phi_0(t) = 0 \quad (14)$$

showing the solution [16]

$$\phi_0(t) \approx e^{-i \frac{F}{\omega^2} \sin(\omega t)}. \quad (15)$$

Injecting this into (10) to get

$$\left\{ \left(-i \frac{\partial}{\partial x} - i \left(k_y - \frac{\partial}{\partial t} \right) \right) \psi_{22}(x) - \left(i \frac{\partial}{\partial t} + E - V(x) \right) \psi_{21}(x) \right\} e^{-i \frac{F}{\omega^2} \sin(\omega t)} e^{-im\omega t} = 0. \quad (16)$$

Generating the Bessel function J_m using the Jacobi-Anger expansion

$$e^{-i \frac{F}{\omega^2} \sin(\omega t)} = \sum_{m=-\infty}^{+\infty} J_m \left(\frac{F}{\omega^2} \right) e^{-im\omega t} \quad (17)$$

and then we show that (16) can be reduced to

$$\sum_{m=-\infty}^{+\infty} \left\{ \left(-i \frac{\partial}{\partial x} - i \left(k_y - \frac{\partial}{\partial t} \right) \right) \psi_{22}(x) - \left(i \frac{\partial}{\partial t} + E - V(x) \right) \psi_{21}(x) \right\} J_m \left(\frac{F}{\omega^2} \right) e^{-im\omega t} = 0. \quad (18)$$

Consequently, we end up with

$$(V(x) - (E + l\omega)) \psi_{21}(x) = -i \left(\frac{\partial}{\partial x} + (k_y - l\omega) \right) \psi_{22}(x). \quad (19)$$

Similarly, we get from (11)

$$(V(x) - (E + l\omega)) \psi_{22}(x) = -i \left(\frac{\partial}{\partial x} - (k_y - l\omega) \right) \psi_{21}(x) \quad (20)$$

Let us make a change to the spinor components to obtain the Schrödinger equation. This is

$$\psi_{21}(x) = \chi_1 + i\chi_2 \quad (21)$$

$$\psi_{22}(x) = \chi_1 - i\chi_2 \quad (22)$$

After substitution in (19-20), we obtain

$$\frac{\partial^2 \chi_1}{\partial x^2} + \left(-i \frac{\partial V(x)}{\partial x} + (k_y - l\omega)^2 + (V(x) - (E + l\omega))^2 \right) \chi_1 = 0 \quad (23)$$

which can be written as Weber's differential equation [28]

$$\frac{\partial^2 \chi_1(z_l)}{\partial z_l^2} + \left(\frac{1}{2} - v_l - \frac{z_l^2}{4} \right) \chi_1(z_l) = 0 \quad (24)$$

where we have set

$$z_l = \sqrt{\frac{2}{\beta}} e^{\frac{i\pi}{4}} (\beta x + E_l) \quad (25)$$

$$v_l = \frac{i}{2\beta} (k_y - l\omega)^2 \quad (26)$$

$$E_l = E + l\omega - V_0. \quad (27)$$

The solution of (24) is given by

$$\chi_1(z_l) = C_{1,l} D_{v_l-1}(z_l) + C_{2,l} D_{-v_l}(-z_l^*) \quad (28)$$

where $C_{1,l}$ and $C_{2,l}$ are two constants. From χ_1 , we derive the second component

$$\chi_2(z_l) = C_{1,l} \frac{\sqrt{2\beta} e^{-i\frac{\pi}{4}}}{k_y - l\omega} D_{v_l}(z_l) + \frac{C_{2,l}}{(k_y - l\omega)} \left(2(\beta x + E_l) D_{-v_l}(-z_l^*) + \frac{\sqrt{2\beta} e^{i\frac{\pi}{4}}}{k_y - l\omega} D_{1-v_l}(-z_l^*) \right). \quad (29)$$

These allow us to express $\psi_{21}(x)$ and $\psi_{22}(x)$ as follows

$$\psi_{21}(x) = C_{1,l} \mu_l^+(x) + C_{2,l} \zeta_l^+(x) \quad (30)$$

$$\psi_{22}(x) = C_{1,l} \mu_l^-(x) + C_{2,l} \zeta_l^-(x) \quad (31)$$

where we have defined

$$\mu_l^\pm(x) = D_{v_l-1}(z_l) \pm \frac{\sqrt{2\beta}}{k_y - l\omega} e^{\frac{i\pi}{4}} D_{v_l}(z_l) \quad (32)$$

$$\zeta_l^\pm(x) = \frac{1}{k_y - l\omega} \left((k_y - l\omega \mp (2i\beta x + 2iE_l)) D_{-v_l}(-z_l^*) \pm \sqrt{2\beta} e^{-i\frac{\pi}{4}} D_{1-v_l}(-z_l^*) \right). \quad (33)$$

Combining all to write the eigenspinors in region 2 as

$$\Psi_2(x, y, t) = e^{ik_y y} \sum_{l=-\infty}^{+\infty} \left[C_{1,l} \begin{pmatrix} \mu_l^+(x) \\ \mu_l^-(x) \end{pmatrix} + C_{2,l} \begin{pmatrix} \zeta_l^+(x) \\ \zeta_l^-(x) \end{pmatrix} \right] \sum_{m=-\infty}^{+\infty} J_m \left(\frac{F}{\omega^2} \right) e^{-i(E+l\omega+m\omega)t}. \quad (34)$$

In the regions 1 and 3 have only pristine graphene, the spinors in both regions written as follows [21]

$$\Psi_1(x, y, t) = e^{ik_y y} \left[\delta_{l,0} \begin{pmatrix} 1 \\ \Lambda_l \end{pmatrix} e^{ik_l x} e^{-iEt} + \sum_{l=-\infty}^{+\infty} r_l \begin{pmatrix} 1 \\ -\Lambda_l^* \end{pmatrix} e^{-ik_l x} e^{-i(E+l\omega)t} \right] \sum_{m=-\infty}^{+\infty} J_m \left(\frac{F}{\omega^2} \right) e^{-im\omega t} \quad (35)$$

$$\Psi_3(x, y, t) = e^{ik_y y} \sum_{m=-\infty}^{+\infty} \left[t_l \begin{pmatrix} 1 \\ \Lambda_l \end{pmatrix} e^{ik_l x} + b_l \begin{pmatrix} 1 \\ -\Lambda_l^* \end{pmatrix} e^{-ik_l x} \right] \delta_{m,l} e^{-i(E+m\omega)t} \quad (36)$$

corresponding to the eigenvalues

$$E + l\omega = s_l \sqrt{k_l^2 + k_y^2} \quad (37)$$

with the reflection r_l and transmission t_l amplitudes, $\Lambda_l = s_l e^{i\phi_l}$, $\phi_l = \tan^{-1} \frac{k_y}{k_l}$, $\delta_{m,l} = J_{m-l}(0)$, $s_l = \text{sgn}(E + l\omega)$ and b_l is null vector.

III. TRANSMISSION PROBABILITIES

To determine the transmission and reflection amplitudes, we use the boundary conditions at the interfaces $x = 0$ and $x = d$

$$\Psi_1(0, y, t) = \Psi_2(0, y, t) \quad (38)$$

$$\Psi_2(d, y, t) = \Psi_3(d, y, t) \quad (39)$$

together with the orthogonality of $e^{im\omega t}$ to end up with four unknown parameters, each one there in an infinity of modes

$$\delta_{m,0} + r_m = \sum_{l=-\infty}^{+\infty} (c_{1,l} \mu_l^+(0) + c_{2,l} \zeta_l^+(0)) J_{m-l} \left(\frac{F}{\omega^2} \right) \quad (40)$$

$$\delta_{m,0} \Lambda_m - r_m \Lambda_m^* = \sum_{l=-\infty}^{+\infty} (c_{1,l} \mu_l^-(x)(0) + c_{2,l} \zeta_l^-(0)) J_{m-l} \left(\frac{F}{\omega^2} \right) \quad (41)$$

$$t_m e^{ik_m d} + b_m e^{-ik_m d} = \sum_{l=-\infty}^{+\infty} (c_{1,l} \mu_l^+(d) + c_{2,l} \zeta_l^+(d)) J_{m-l} \left(\frac{F}{\omega^2} \right) \quad (42)$$

$$t_m \Lambda_m e^{ik_m d} - b_m \Lambda_m^* e^{-ik_m d} = \sum_{l=-\infty}^{+\infty} (c_{1,l} \mu_l^-(d) + c_{2,l} \zeta_l^-(d)) J_{m-l} \left(\frac{F}{\omega^2} \right) \quad (43)$$

These relations can be expressed using the transfer matrix approach to connect the three regions of the system under consideration. This is

$$\begin{pmatrix} \Gamma_1 \\ \Gamma_1' \end{pmatrix} = \mathbb{M} \begin{pmatrix} \Gamma_2 \\ \Gamma_2' \end{pmatrix} \quad (44)$$

with the total transfer matrix

$$\mathbb{M} = \begin{pmatrix} M_{1,1} & M_{1,2} \\ M_{2,1} & M_{2,2} \end{pmatrix} = \mathbb{M}(0, 1) \cdot \mathbb{M}(1, 2) \quad (45)$$

where $\mathbb{M}(j, j+1)$ is the transfer matrix connecting regions j and $j+1$

$$\mathbb{M}(0, 1) = \begin{pmatrix} \mathbb{I} & \mathbb{I} \\ \mathbb{S}^+ & \mathbb{S}^- \end{pmatrix}^{-1} \begin{pmatrix} \mathbb{F}_0^+ & \mathbb{R}_0^+ \\ \mathbb{F}_0^- & \mathbb{R}_0^- \end{pmatrix} \quad (46)$$

$$\mathbb{M}(1, 2) = \begin{pmatrix} \mathbb{F}_d^+ & \mathbb{R}_d^+ \\ \mathbb{F}_d^- & \mathbb{R}_d^- \end{pmatrix}^{-1} \begin{pmatrix} \mathbb{I} & \mathbb{I} \\ \mathbb{S}^+ & \mathbb{S}^- \end{pmatrix} \begin{pmatrix} \mathbb{Q}^+ & \mathbb{O} \\ \mathbb{O} & \mathbb{Q}^- \end{pmatrix} \quad (47)$$

and the quantities

$$\mathbb{S}^\pm = \pm \delta_{m,l} \Lambda_l^{\pm 1}, \quad \mathbb{F}_z^\pm = \mu_l^\pm(z) J_{m-l} \left(\frac{F}{\omega^2} \right) \quad (48)$$

$$\mathbb{R}_z^\pm = \zeta_l^\pm(z) J_{m-l} \left(\frac{F}{\omega^2} \right), \quad \mathbb{Q}^\pm = e^{\pm i k_l L} \delta_{m,l} \quad (49)$$

where \mathbb{O} is the zero matrix, \mathbb{I} is the unit matrix and $z = \{0, d\}$. We consider the fermions moving from left to right with the energy E , then from Eq. (44) we get

$$\Gamma_2 = \mathbb{M}_{1,1}^{-1} \Gamma_1 \quad (50)$$

where $\Gamma_1 = \delta_{0,l}$ is the Kronecker symbol and $\Gamma_2 = t_l$. Because n, l varies from $-\infty$ to $+\infty$, the transfer matrix approach, which we determined above, is of infinite order, making it difficult to solve. To accomplish this, we replace the infinite series with a finite number of terms ranging from $-N$ to N , where $N > \frac{F}{\omega^2}$, and we limit ourselves only to the first energy side bands $E \pm m\omega$, yielding the result

$$t_{-N+k} = M'[k+1, N+1] \quad (51)$$

with $M' = M_{1,1}^{-1}$ and $k = 0, 1, 2, \dots, N$.

On the other hand, the transmission probability can be expressed by using the continuity equation. According to our Hamiltonian, the general expression of the current density takes the following form:

$$J = \Psi_j^*(x, y, t) \sigma_x \Psi_j(x, y, t) \quad (52)$$

which makes it possible to determine the current densities in each region j . There are given by

$$J_{in,0} = (\Lambda_0 + \Lambda_0^*) \quad (53)$$

$$J_{re,l} = r_l^* r_l (\Lambda_l + \Lambda_l^*) \quad (54)$$

$$J_{tr,l} = t_l^* t_l (\Lambda_l + \Lambda_l^*). \quad (55)$$

Then by using the relations

$$T_l = \frac{|J_{tr,l}|}{|J_{in,0}|}, \quad R_l = \frac{|J_{re,l}|}{|J_{in,0}|} \quad (56)$$

one can express of the transmission T_l and reflection R_l probabilities as

$$T_l = s' \frac{\cos \theta_l}{\cos \theta_0} |t_l|^2, \quad R_l = s' \frac{\cos \theta_l}{\cos \theta_0} |r_l|^2 \quad (57)$$

where the two angles are

$$\cos \theta_l = \frac{k_l}{\sqrt{k_l^2 + k_y^2}}, \quad \cos \theta_0 = \frac{k_0}{\sqrt{k_0^2 + k_y^2}} \quad (58)$$

and the sign is $s' = s_l s_0$.

To simplify the numerical calculation, we pronounce only the first sidebands, i.e. $l = -1, 0, 1$. The corresponding transmissions are

$$t_{-1} = M'[1, 2] \quad (59)$$

$$t_0 = M'[2, 2] \quad (60)$$

$$t_1 = M'[3, 2]. \quad (61)$$

In the following section, we will plot the transmission probability as a function of the current system's physical parameters for the three first bands: the central band ($l = 0$) and the two first side bands ($l = \pm 1$). We will analyze them to demonstrate the effect of the barrier that we applied on the movement of the Dirac fermions.

IV. NUMERICAL RESULTS

Fig. 2 represents the transmission probabilities as a function of the incident energy E . The total transmission $T = T_0$ (magenta line) is shown in Fig. 2a, and the other bands $T_{\pm 1}$ are zero in the absence of laser irradiation $F = 0$ of a linear barrier ($V_0 = 20, V_1 = 0$). Let us now examine what happens in the intermediate region if laser irradiation $F = 0.9$ is introduced, as shown by the transmission for the central band T_0 (blue line) and the two first sidebands T_{-1} (red line) and T_1 (green line). We also find that the laser irradiation is very significant in determining the relative transmission probabilities of two first sidebands. Transmissions are prohibited for the energy color red, $E = \pm\omega$, resulting in a change in k_y to $k_y \pm \omega$, which serves as an effective mass m^* [25, 29]. The total transmission and the transmission of the central band oscillate around a minimum for the energies EV_0 , then increase passing by EV_0 up to a maximum value, and the total transmission (the sum of the three) tends towards 1, indicating that our system exhibits classic behavior after the barrier, indicating the presence of the Klein effect. The same transmissions are plotted in Fig. 2b, but with a two-potential barrier ($V_0 = 20, V_1 = 15$). The transmission of the central band is more dominant in the energy zone $k_y < E < V_1$, and the total transmission oscillates in the neighborhood of 1. The Klein paradox is always present. We observe a total reflection in the energy zone $V_1 < E < V_0$, with a very small transmission for the band corresponding to $l = 1$. In the third zone, $E > V_1$, total transmission rapidly decreases towards unit, and T_0 increases with an apparent oscillation. Finally, we see that changing the barrier's inclination coefficient, $\beta = \frac{V_0 - V_1}{d}$, affects the shape of the transmissions and the number of oscillations.

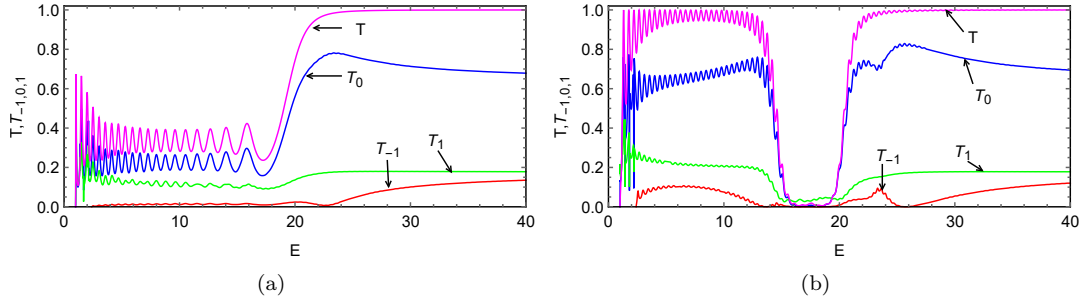


FIG. 2. (Color online) Transmission probabilities as a function of the incident energy E with $d = 7, V_0 = 20, k_y = 1, \omega = 1.4, F = 0$ for T (magenta line), $F = 0.9$ for the central transmission band T_0 (blue line) and two first sidebands T_{-1} (red line), T_1 (green line). (a): $V_1 = 0$ and (b): $V_1 = 15$.

Fig. 3 illustrates the transmission of the central band ($l = 0$) as a function of the incident energy E with $d = 7, V_0 = 20, V_1 = 15, k_y = 1$ for $\omega = 1.4, F = \{0.2, 0.9, 1.8\}$ in Fig. 3a and $F = 1.8, \omega = \{1.5, 2, 2.5\}$ in Fig. 3b. They show that the transmission probability varies in an oscillatory way, and guards even allure, but with an attenuation proportional to F and ω , and oscillations appear after the barrier. The oscillation becomes important when F increases, as shown in Fig. 3a, but it also becomes important when ω decreases, as shown in Fig. 3b. Finally, the ratio $\frac{F}{\omega^2}$ is important because it determines the shape, amplitude, and oscillations of the transmission probability. Inside the barrier, we always have a total reflection for all values of ω and F .

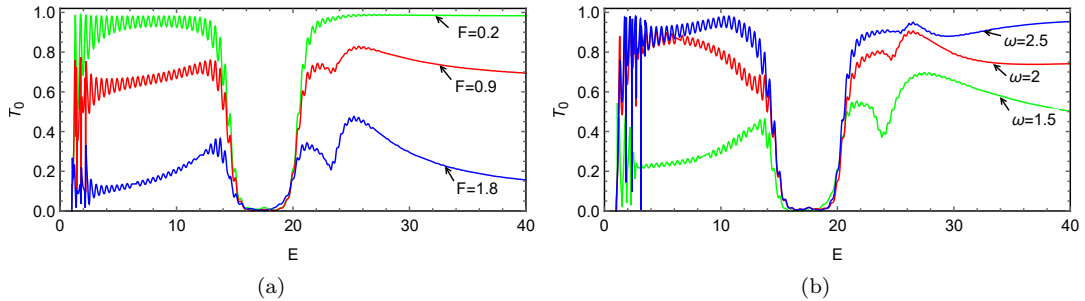


FIG. 3. (Color online) Transmission probability for the central band T_0 as a function of the incident energy E with $d = 7, V_0 = 20, V_1 = 15, k_y = 1$. (a): $\omega = 1.4, F = 0.2$ (green color), $F = 0.9$ (red line) and $F = 1.8$ (blue line). (b): $F = 1.8, \omega = 1.5$ (green color), $\omega = 2$ (red line) and $\omega = 2.5$ (blue line).

Fig. 4 depicts transmissions as a function of the barrier potential V_1 under various conditions. Taking $\omega = 1.4$ and $F = 0.9$ in Fig. 4a, we can see that transmissions decrease from zero to $E - 2k_y$, then increase to $E + 2k_y$. When $V_1 > E + 2k_y$, the transmissions are maximized, and we have a total transmission. Fig. 4b depicts the transmission T_1 as a function of V_1 with varying ω and F values. We observe that when the ratio $\frac{F}{\omega^2}$ decreases, the amplitude of T_1 also decreases. The green line corresponds to $\frac{F}{\omega^2} = 0.91$ and the blue line corresponds to $\frac{F}{\omega^2} = 0.2$. As a result, we note that the ratio $\frac{F}{\omega^2}$ plays an important role in increasing or decreasing the amplitude of the transmissions.

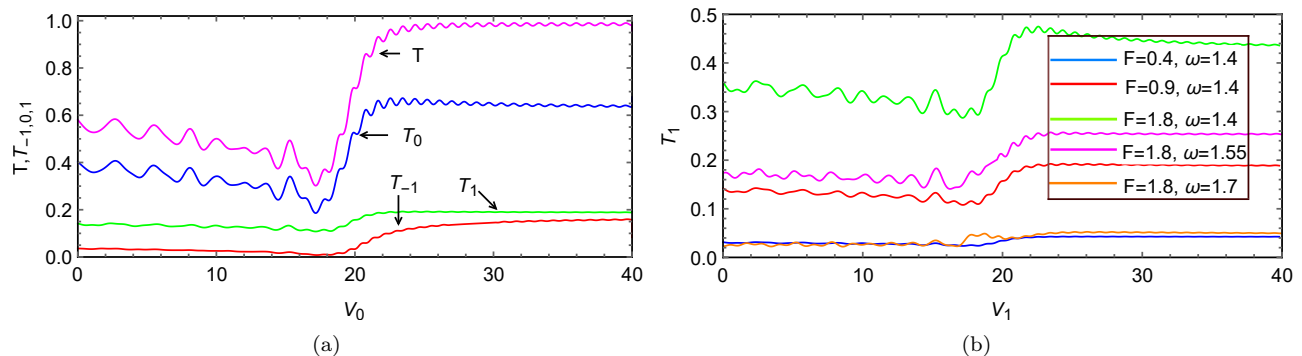


FIG. 4. (Color online) Transmission probabilities as a function of potential V_1 with $d = 7$, $V_0 = 40$, $E = 20$, $k_y = 1$. (a): $\omega = 1.4$, $F = 0.9$ for the total transmission T (magenta line), the central transmission band T_0 (blue line) and two first sidebands T_{-1} (red line), T_1 (green line). (b): Transmission probability T_1 with $\{F = 0.4, \omega = 1.4\}$ (blue line), $\{F = 0.9, \omega = 1.4\}$ (red line), $\{F = 1.8, \omega = 1.4\}$ (green line), $\{F = 1.8, \omega = 1.55\}$ (magenta line), $\{F = 1.8, \omega = 1.7\}$ (orange line).

Fig. 5 shows the transmission probabilities as a function of the barrier potential V_0 with $d = 7$, $V_1 = 0$, $E = 20$ and $k_y = 1$. When we use $\omega = 1.4$ and $\frac{F}{\omega^2} = 0.46$ in Fig. 5a, we see that T_0 is always more dominant, and T for $V_1 < E - 2k_y$ is nearly equal to 1 (Klein zone). Both T_0 and T decrease from $E - 2k_y$ to $E + 2k_y$, then increase in an oscillatory way. In Fig. 5b, we only show T_{-1} as a function of V_1 with different ω values. The amplitude and shape of T_{-1} are clearly dependent on the parameters ω and F . Indeed, the amplitude is maximum and greater than 0.25 for $\frac{F}{\omega^2} = 0.91$ (blue line), then it rapidly decreases to zero after increasing in an oscillatory manner. The amplitude increases up to a maximum greater than 0.2 for $\frac{F}{\omega^2} = 0.55$ (red line), then rapidly decreases to zero. For $\frac{F}{\omega^2} = 0.26$ (green line), the amplitude does not exceed 0.05 then it decreases to zero. It can be concluded that the potential and the laser field parameters have a direct effect on all transmissions.

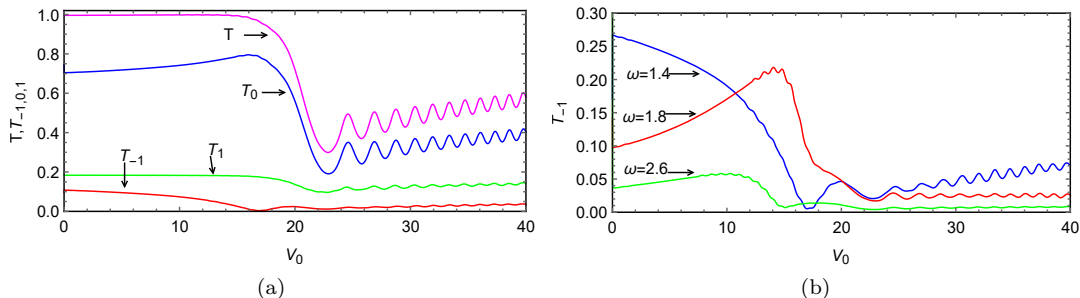


FIG. 5. (Color online) Transmission probabilities as a function of potential V_0 with $d = 7$, $V_1 = 0$, $E = 20$, $k_y = 1$. (a): $\omega = 1.4$, $F = 0.9$ for total transmission T (magenta line), the central transmission band T_0 (blue line) and two first sidebands T_{-1} (red line), T_1 (green line). (b): Transmission probability T_{-1} with $F = 1.8$, $\omega = 1.4$ (blue line), $\omega = 1.8$ (red line) and $\omega = 2.6$ (green line).

The transmission probabilities for the first three bands are shown in Fig. 6 as a function of barrier width d , with $V_0 = 20$, $V_1 = 10$, $E = 5$, $k_y = 1$, and $\omega = 1.4$. In Fig. 6a, for $F = 0.9$, we observe that all transmissions oscillate in a sinusoidal manner with the same period but different amplitudes, indicating a large difference between T_0 and $T_{-1,1}$. The transmission T_0 is always more dominant, and it oscillates in the vicinity of 1. When we plotted the same transmissions for $F = 1.8$, we saw that their nature remained the same, but their amplitudes grew larger without the spacing between T_0 and $T_{-1,1}$, as shown in Fig. 6b. The amplitude of T_0 decreases and that of $T_{-1,1}$ increases

along the d axis, but the sum of the three transmissions, $T_{-1,0,1}$, would never exceed unity, which indicates that the transmission in the central band is important for short barriers. However, side band transmissions become important for large barriers. We conclude that the laser parameters have an effect on the amplitudes and the nature of the transmission probabilities.

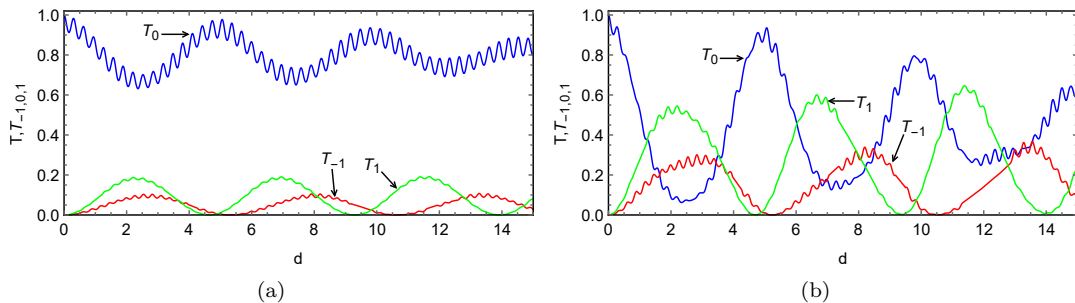


FIG. 6. (Color online) Transmission probabilities for the central band T_0 (blue line) and two first sidebands T_{-1} (red line), T_1 (green line) as a function of the barrier width d with $V_0 = 20$, $V_1 = 10$, $E = 5$, $k_y = 1$. $\omega = 1.4$. (a): $F = 0.8$ and (b): $F = 1.8$.

V. CONCLUSION

We theoretically investigated a system consisting of three graphene regions: 1, 2, 3, virgin graphene, and an intermediate region with a laser field generated by an electric field of amplitude F and frequency ω in the presence of an inclined scalar potential generated between two identical plates by two different potential generators V_0, V_1 . First, we solved the eigenvalue equation to determine the wave functions corresponding to each region. For this, we used the Floquet's theory and the solution of Weber's differential equation. To determine the transmission probabilities, we employed the boundary conditions and used transfer matrix approach, which give an infinite order transfer matrix. To simplify, we limited our studies to the first three bands, that are the central band $l = 0$ and the two first side bands $l = \pm 1$.

We plotted the transmission probabilities as a function of the physical parameters E , V_0 , V_1 , d , and ω . In summary, our numerical results showed that the laser field plays an important role in the barrier. The oscillations of this barrier over time generate several modes of transmission probabilities. It is demonstrated that the reflection is complete inside the barrier for all modes. It is found that the variation of the frequency ω or the amplitude F (i.e. $\frac{F}{\omega^2}$) changes the form and the amplitude of transmissions. More importantly, we observed that the transmission of the central band is always more dominant than the sidebands, and the Klein zone is always present, especially for energies lower than the barrier potential.

-
- [1] K. S. Novoselov, A. K. Geim, S. V. Morozov, D. Jiang, Y. Zhang, S. V. Dubonos, I. V. Grigorieva, and A. A. Firsov, *Science* 306, 666 (2004).
 - [2] K. S. Novoselov, A. K. Geim, S. V. Morozov, D. Jiang, M. I. Katsnelson, I. V. Grigorieva, S. V. Dubonos, and A. A. Firsov, *Nature* 438, 197 (2005).
 - [3] A. H. Castro Neto, F. Guinea, N. M. R. Peres, K. S. Novoselov, and A. K. Geim, *Rev. Mod. Phys.* 81, 109 (2009).
 - [4] S. Bhattacharjee and K. Sengupta, *Phys. Rev. Lett.* 97, 217001 (2006).
 - [5] J. S. Bunch, Y. Yaish, M. Brink, K. Bolotin, and P. L. McEuen, *Nano Lett.* 5, 2887 (2005).
 - [6] Claire Berger, Zhimin Song, Tianbo Li, Xuebin Li, Asmerom Y. Ogbazghi, Rui Feng, Zhenting Dai, Alexei N. Marchenkov, Edward H. Conrad, Phillip N. First, and Walt A. de Heer, *J. Phys. Chem. B* 108, 19912 (2004).
 - [7] Y. Zhang, Y. W. Tan, H. L. Stormer, and P. Kim, *Nature* 438, 201 (2005).
 - [8] S. V. Morozov, K. S. Novoselov, F. Schedin, D. Jiang, A. A. Firsov, and A. K. Geim, *Phys. Rev. B* 72, 201401 (2005).
 - [9] H. Haugen, D. Huertas-Hernando, A. Brataas, *Phys. Rev. B* 77, 115406 (2008).
 - [10] Z. H. Ni, T. Yu, Y. H. Lu, Y. Y. Wang, Y. P. Feng, and Z. X. Shen, *ACS Nano* 2, 2301 (2008).
 - [11] M. Y. Huang, H. G. Yan, C. Y. Chen, D. H. Song, T. F. Heinz, and J. Hone, *Proc. Natl. Acad. Sci. U.S.A.* 106, 7304 (2009).
 - [12] Y. Zahidi, I. Redouani, A. Jellal, and Hocine Bahlouli, *Physica E* 115, 113672 (2020).
 - [13] H. Bahlouli, E. B. Choubabi, A. El Mouhafid, and A. Jellal, *Solid State Communications* 151, 1309 (2011).
 - [14] M. Mekkaoui, A. Jellal, and H. Bahlouli, *Solid State Communications* 358, 114981 (2022).

- [15] C. Sinha and R. Biswas, *Appl. Phys. Lett.* 100, 183107 (2012).
- [16] R. Biswas and C. Sinha, *Appl. Phys.* 114, 183706 (2013).
- [17] R. El Aitouni and A. Jellal, *Phys. Lett. A.* 447, 128288 (2022).
- [18] H. L. Calvo, H. M. Pastawski, S. Roche, and L. E. F. Torres, *Appl. Phys. Lett.* 98, 232103 (2011).
- [19] S. E. Savel'ev and A. S. Alexandrov, *Phys Rev. B.* 84, 035428 (2011).
- [20] J. T. Lu, F. H. Su, H. Wang, and X. H. Deng, *Europhys. Lett.* 95, 24003 (2011).
- [21] M. Mekkaoui, R. El Kinani, and A. Jellal, *Mater. Res. Express* 6, 085013 (2019).
- [22] C. W. J. Beenakker, *Rev. Mod. Phys.* 80, 1337 (2008).
- [23] M. I. Katsnelson, K. S. Novoselov, A. K. Geim, *Nat. Phys.* 2, 620 (2006).
- [24] R. Biswas, S. Maitty, and C. Sinha, *Physica E* 84, 235 (2016).
- [25] E. Choubabi, A. Jellal, and M. Mekkaoui, *Eur. Phys. J. B* 92, 1 (2019).
- [26] R. Loudon, *The Quantum Theory of Light*, 3rd ed. (Oxford University Press Inc, New York, 2000).
- [27] Z. Gu, H. A. Fertig, D. P. Arovas, and A. Auerbach, *Phys. Rev. Lett.* 107, 216601 (2011).
- [28] F. W. J. Olver, *J. Res. Nat. Bur. Standards B* 63, 131 (1959).
- [29] A. Jellal, E. B. Choubabi, H. Bahlouli, and A. Aljaafari, *J. Low Temp. Phys.* 168, 40 (2012).